JOURNAL OF GUIDANCE, CONTROL, AND DYNAMICS
Vol. 28, No. 4, July–August 2005

Dynamic Stability of Electrodynamic Tethers in Inclined Elliptical Orbits

J. Peláez*
Technical University of Madrid, E-28040 Madrid, Spain
and
Y. N. Andrés†
ESA, D-64293 Darmstadt, Germany

For a circular orbit, the local vertical rotates uniformly about the orbit normal, and it is a stable equilibrium position for, basically, any tether. For an elliptical orbit, however, the local vertical does not rotate uniformly, and it is no longer an equilibrium position for the tether: the librations dynamics become excited even if the tether is left at rest along the local vertical. Instead of stable equilibrium positions, the governing equations have periodic solutions. For an electrodynamic tether, the equilibrium positions along the local vertical do not exist even in the circular case. Using simple models to describe the Earth magnetic field and the tether current, the governing equations also have periodic solutions instead of equilibrium positions. The goal of this paper is to analyze the combined action of these two forcing terms: the eccentricity of the orbit and the electrodynamic forces. The joint influence of both effects give place to new periodic solutions, which play an essential role. They are detected, and their stability properties are analyzed because they provide the system dynamic stability.

Introduction

RECENTLY a new kind of dynamic instability has been addressed for electrodynamic tethers operating in inclined, circular orbits (see Refs. 1–4). Using simple models (a nontilted dipole model for the Earth magnetic field, a tether current that does not change along the orbit, and a dumbbell model for the tether), the system governing equations are forced periodically by the electromagnetic terms that have the orbital period. Independently of the model (flexible or rigid) used to describe the tether dynamics, this instability appears in the motion relative to the system center of mass G, when the orbital inclination is not zero. In addition to the inclination, there is a nondimensional parameter ε, defined in Eq. (18), which gauges the electrodynamic torque vs the torque produced by the gravity gradient and inertia forces. Thus, when ε is zero the system has stable equilibrium positions with the tether along the local vertical, but for $\varepsilon \neq 0$ the governing equations have periodic solutions instead. Because of the frequency entrainment, these periodic solutions have the orbital period or an integer multiple of it. Previous analyses have been made for a circular orbit by using asymptotic techniques when $\varepsilon \ll 1$ and numerical procedures when $\varepsilon \approx \mathcal{O}(1)$ (Refs. 1–3). In those papers, the existence of a special periodic solution with the orbital period, which reduces to the stable equilibrium position when ε goes to zero, was shown. However, in the absence of damping or control this periodic solution is unstable. This instability plays an important role in the motion of the tether relative to the system center of mass. A similar situation appears with models that account for the electrodynamic forces in a more elaborated way.[5]

Elliptical orbits have been used in many space missions from very early on. For a satellite in elliptic orbit, the stability of its attitude motion becomes an important dynamical issue. It is well known that gravity-gradient-oriented satellites in circular orbit have equilibrium positions relative to the orbital frame. In these positions, the principal axes of inertia of the satellite coincide with the axes of the frame. Some of these equilibria are stable. Unfortunately, the equilibrium positions disappear when the satellite follows an elliptical orbit. The works of Modi and Brereton[6,7] show that, in place of the equilibrium positions, periodic solutions appear and the satellite dynamics become more complex.

In a tethered satellite, the gravity-gradient stabilization is strong because tethers are usually very long. In the stable equilibrium position, the tether remains aligned with the local vertical. However, when the system center of mass follows an elliptical orbit the tether oscillates around the local vertical, and if the orbit eccentricity is sufficiently large the oscillation becomes a rotation.

For an elliptical orbit, the equations governing the motion relative to the system center of mass can be rewritten, introducing the effects of the eccentricity as periodic forcing terms, which change with the orbital period and vanish when the orbital eccentricity goes to zero. This way, the ellipticity of the orbit causes a perturbation of the librations that take place in the circular case.

The goal of this paper is to analyze the effects of the combined action of two forcing terms: the eccentricity of the orbit and the electrodynamic forces. Four free parameters appear in the problem: the eccentricity e, the orbital inclination i, the argument of the perigee ω, and the just-mentioned parameter ε. At first sight, the eccentricity could reinforce the instability caused by the electrodynamic forces. However, other possibilities cannot be ruled out: the instability could become smoother because of the eccentricity in some range of values of the parameters. In any case, it would be necessary to clarify this point with a detailed analysis that will consist of three logical stages:

1) First, we analyze the dynamics when the tether follows an elliptical orbit ($e \neq 0$) without electrodynamic forces ($\varepsilon = 0$). Some families of periodic orbits are obtained. As a part of the analysis, the linear stability properties of these periodic solutions will be determined, showing the influence of the eccentricity on the eigenvalues of the monodromy matrix of the periodic solutions.

2) In the second stage, the influence of the electrodynamic forces $\varepsilon \neq 0$ will be considered.

3) Finally, the comparison with the circular case will be detailed.

The first stage has no new results. The periodic solutions involved have been obtained in Ref. 6 and their stability properties analyzed

Presented as Paper AAS 03-538 at the AAS/AIAA Astrodynamics Specialists Conference, Big Sky, MT, 3–7 August 2003; received 24 November 2003; revision received 11 August 2004; accepted for publication 2 September 2004.

*E.T.S.I. Aeronáuticos, Pza. Cardenal Cisneros 3; jpelaez@faia.upm.es.
†GMV S.A. based at ESA/European Space Operations Centre, Robert-Bosch-Str. 5; Yago.Andres@esa.int.

in Ref. 7. Therefore, these results have been well known for some time. In this paper, they will be obtained again by using a different approach more convenient for the subsequent analysis. We use a numeric algorithm based on the Poincaré method of continuation of periodic orbits, which provides both the periodic orbits of each family and their stability properties, as functions of the orbit eccentricity. The fundamentals of the algorithm can be found in Ref. 8.

Dumbbell Model

Let $Ex_1y_1z_1$ be the geocentric inertial frame. Its origin E is the Earth center of mass, the axis Ex_1 points to the first Aries point, the axis Ey_1 is in the equatorial plane, and the coordinate system is right-hand oriented. We try to describe the motion of the system relative to this frame.

We will use simple models to underline the physical effects involved in the problem. We consider a system formed by two end masses joined by a rigid rod of length L and mass m_t, aligned with the unit vector $\boldsymbol{u}$ (Fig. 1). The upper mass will be m_2 and the lower one m_1. The center of mass G of the system follows a Keplerian orbit with eccentricity e and inclination i. Instead of (m_1, m_2, m_t), the mass geometry of the system is described in a better way with three different parameters (m, ϕ, Λ_t). The total mass of the system is $m = m_1 + m_2 + m_t$, and $\Lambda_t = m_t/m$ is the fraction of the total mass by the tether mass. Both end masses can be described by using the parameter ϕ defined by

$$\cos^2\phi = (1/m)\left\{m_1 + \tfrac{1}{2}m_t\right\} \Rightarrow m_1 = m\left(\cos^2\phi - \tfrac{1}{2}\Lambda_t\right) \quad (1)$$

$$\sin^2\phi = (1/m)\left\{m_2 + \tfrac{1}{2}m_t\right\} \Rightarrow m_2 = m\left(\sin^2\phi - \tfrac{1}{2}\Lambda_t\right) \quad (2)$$

The maximum (minimum) value of ϕ corresponds to $m_1 = 0$ ($m_2 = 0$), respectively. Thus, $\phi \in [\phi_{\min}, \phi_{\max}]$, and the ends of this interval only depend on Λ_t

$$\phi_{\min} = \arcsin\left(\sqrt{\Lambda_t/2}\right) \qquad (m_2 = 0)$$

$$\phi_{\max} = \arccos\left(\sqrt{\Lambda_t/2}\right) \qquad (m_1 = 0)$$

If $\Lambda_t = 0$, $\phi_{\min} = 0$, and $\phi_{\max} = \pi/2$. For fixed values of Λ_t and m, when ϕ describes the interval $[\phi_{\min}, \phi_{\max}]$ from the lower to the upper end, mass is re-distributed from the lower particle to the upper one. The total mass m does not change in this process. Then, $\phi = \pi/4$ if both end masses are equal.

The position of the center of mass G and the moment of inertia relative to a line perpendicular to the tether through G are

$$h_G = L\cos^2\phi, \qquad I_s = (1/12)mL^2\left(3\sin^2 2\phi - 2\Lambda_t\right) \quad (3)$$

Because we are dealing with a rigid body, we separate the motion of the center of mass G from the attitude dynamics problem.

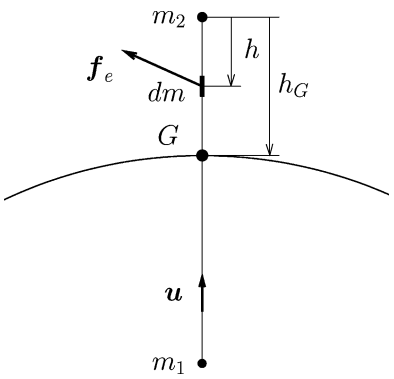

Fig. 1 Mass distribution of the system.

Motion of the Center of Mass

The only forces that we consider in the problem are the gravitational and electrodynamic forces. We assume that m, the total mass of the system, is large. As a consequence, the orbit decay rate produced by the electrodynamic drag is negligible. Moreover, the gravitational forces do not produce, on average, decay of the orbit. Thus, we will assume that the center of mass of the system follows an unperturbed Keplerian ellipse. Taking polar coordinates (r, ν) inside the orbital plane, the equation of the orbit will be

$$r = \frac{a(1-e^2)}{1 + e\cos\nu} \quad (4)$$

where ν is the true anomaly, measured from the perigee.

Attitude Dynamics

Let $Gx_1y_1z_1$ be a movable frame with origin in the system center of mass G and whose axes remain parallel to the corresponding axes of the geocentric inertial frame $Ex_1y_1z_1$. By definition, the motion relative to the system center of mass G is the motion of the system relative to the frame $Gx_1y_1z_1$, and it is governed by the angular momentum equation

$$\frac{\mathrm{d}}{\mathrm{d}t}(\boldsymbol{H}_G) = \boldsymbol{M}_G + \boldsymbol{M}_E \quad (5)$$

where $\boldsymbol{H}_G$ is the angular momentum of the system given by $\boldsymbol{H}_G = \bar{\bar{I}}_G \circ \boldsymbol{\omega}$. Here $\bar{\bar{I}}_G$ is the central inertia tensor and $\boldsymbol{\omega}$ is the angular velocity relative to the frame $Gx_1y_1z_1$, and it takes the value

$$\boldsymbol{\omega} = \boldsymbol{u} \times \dot{\boldsymbol{u}} + \alpha\boldsymbol{u} \quad (6)$$

[In Eq. (6), the particular value of α is irrelevant because the moment of inertia relative to the tether line vanishes.] On the right-hand side of Eq. (5), we find the gravitational torque $\boldsymbol{M}_G$ and the electrodynamic torque $\boldsymbol{M}_E$. Both act in the system center of mass G. We will give expressions for these two torques shortly [Eqs. (10) and (11)].

Because $(\boldsymbol{u} \times \dot{\boldsymbol{u}})$ lies in a principal direction of inertia in G, the following relation holds:

$$\bar{\bar{I}}_G \circ \boldsymbol{\omega} = \bar{\bar{I}}_G \circ (\boldsymbol{u} \times \dot{\boldsymbol{u}}) + \bar{\bar{I}}_G \circ (\alpha\boldsymbol{u}) = I_s(\boldsymbol{u} \times \dot{\boldsymbol{u}})$$

Thus, Eq. (5) takes the form

$$\boldsymbol{u} \times \ddot{\boldsymbol{u}} = (1/I_s)(\boldsymbol{M}_G + \boldsymbol{M}_E) \quad (7)$$

The derivative $\ddot{\boldsymbol{u}}$ must be calculated in the inertial frame, where the unit vectors $(\boldsymbol{i}_1, \boldsymbol{j}_1, \boldsymbol{k}_1)$ remain fixed.

We will introduce the orbital frame $Gxyz$, with origin at the system center of mass G, the Gx axis along the local vertical pointing to zenith and the Gy axis normal to the orbital plane (Fig. 2). The position of the tether and its unit vector $\boldsymbol{u}$ is defined by the in-plane angle θ and the out-of-plane angle φ

$$\boldsymbol{u} = \cos\varphi\cos\theta\boldsymbol{i} - \sin\varphi\boldsymbol{j} + \cos\varphi\sin\theta\boldsymbol{k}$$

In what follows, the Coriolis theorem

$$\left.\frac{\mathrm{d}\boldsymbol{A}(t)}{\mathrm{d}t}\right|_{(1)} = \left.\frac{\mathrm{d}\boldsymbol{A}(t)}{\mathrm{d}t}\right|_{(0)} + \boldsymbol{\omega}_{\mathcal{R}} \times \boldsymbol{A}(t)$$

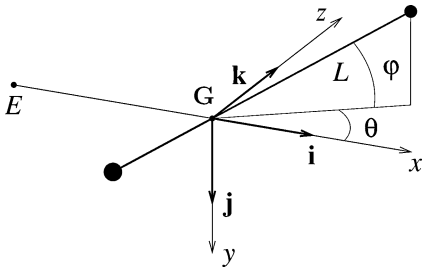

Fig. 2 Orbital frame and tether position.

relating the time derivative of a given vector $\boldsymbol{A}(t)$ in the geocentric inertial frame (body 1) and the time derivative in the orbital frame (body 0) will be used. In this expression, $\boldsymbol{\omega}_{\mathcal{R}} = -\dot{\nu}\boldsymbol{j}$ is the angular velocity of the orbital frame relative to the inertial frame. This way, we get

$$\ddot{\boldsymbol{u}} = \boldsymbol{u}'' + \boldsymbol{\alpha}_{\mathcal{R}} \times \boldsymbol{u} + 2\boldsymbol{\omega}_{\mathcal{R}} \times \boldsymbol{u}' + \boldsymbol{\omega}_{\mathcal{R}} \times (\boldsymbol{\omega}_{\mathcal{R}} \times \boldsymbol{u}) \tag{8}$$

where $\boldsymbol{u}'$ and $\boldsymbol{u}''$ are the time derivatives of $\boldsymbol{u}$ in the orbital frame, and $\boldsymbol{\alpha}_{\mathcal{R}} = -\ddot{\nu}\boldsymbol{j}$ is the angular acceleration of the orbital frame relative to the inertial frame. Equation (7) takes the form

$$\boldsymbol{u} \times \boldsymbol{u}'' = (1/I_s)(\boldsymbol{M}_G + \boldsymbol{M}_E) - \boldsymbol{u} \times (\boldsymbol{\alpha}_{\mathcal{R}} \times \boldsymbol{u}) + 2(\boldsymbol{\omega}_{\mathcal{R}} \cdot \boldsymbol{u})\boldsymbol{u}' - (\boldsymbol{u} \times \boldsymbol{\omega}_{\mathcal{R}})(\boldsymbol{u} \cdot \boldsymbol{\omega}_{\mathcal{R}}) \tag{9}$$

The gravitational torque is given by

$$\boldsymbol{M}_G \approx (3\mu/r^3)\boldsymbol{i} \times (\bar{\bar{\boldsymbol{I}}}_G \circ \boldsymbol{i})$$

where μ is the Earth gravitational constant. To obtain this expression, some assumptions have been made: 1) the Earth gravitational field is perfectly spherical, and 2) when compared with unity, terms of order L/r—and higher—have been neglected.

The identity $\boldsymbol{i} = (\boldsymbol{i} \cdot \boldsymbol{u})\boldsymbol{u} + \boldsymbol{u} \times (\boldsymbol{i} \times \boldsymbol{u})$ leads to

$$\bar{\bar{\boldsymbol{I}}}_G \circ \boldsymbol{i} = I_s \boldsymbol{u} \times (\boldsymbol{i} \times \boldsymbol{u}) = I_s[\boldsymbol{i} - \boldsymbol{u}(\boldsymbol{i} \cdot \boldsymbol{u})]$$

and the gravitational torque turns out to be

$$\boldsymbol{M}_G \approx (3\mu/r^3) I_s (\boldsymbol{u} \times \boldsymbol{i})(\boldsymbol{u} \cdot \boldsymbol{i}) \tag{10}$$

The torque about G introduced by the electrodynamic forces is

$$\boldsymbol{M}_E = \boldsymbol{u} \times (\boldsymbol{u} \times \boldsymbol{B}) J_1, \quad \text{where} \quad J_1 = \int_0^L (h_G - h) I_e(h)\, \mathrm{d}h \tag{11}$$

$I_e(h)$ is the tether current profile, and $\boldsymbol{B}$ is the Earth magnetic field, which will be considered constant along the tether (and equal to its value in G). To model the magnetic field $\boldsymbol{B}$, a nontilted dipole model will be used. The components (B_x, B_y, B_z) in the orbital frame of the magnetic field are

$$B_x = -\left(2\mu_m / r^3\right) \sin i \sin(\omega + \nu), \qquad B_y = -\left(\mu_m / r^3\right) \cos i$$

$$B_z = +\left(\mu_m / r^3\right) \sin i \cos(\omega + \nu)$$

In these expressions, ω is the argument of the perigee, and μ_m the intensity of the magnetic dipole. The details can be found in Refs. 1 and 2.

Governing Equations

The vectorial equation (9) provides two scalar relations when projected onto two independent directions different from the tether line (projecting onto the tether line leads to the trivial identity).

Let $\boldsymbol{u}_2$ be a unit vector lying in the orbital plane and perpendicular to the tether line. Projecting onto the vectors $\boldsymbol{j}$ and $\boldsymbol{u}_2$, we get the equations

$$\boldsymbol{j} \cdot (\boldsymbol{u} \times \boldsymbol{u}'') = \boldsymbol{j} \cdot [(1/I_s)(\boldsymbol{M}_G + \boldsymbol{M}_E) - \boldsymbol{P}] \tag{12}$$

$$\boldsymbol{u}_2 \cdot (\boldsymbol{u} \times \boldsymbol{u}'') = \boldsymbol{u}_2 \cdot [(1/I_s)(\boldsymbol{M}_G + \boldsymbol{M}_E) - \boldsymbol{P}] \tag{13}$$

where $\boldsymbol{P}$ is a vectorial expression given by

$$\boldsymbol{P} = -\boldsymbol{u} \times (\boldsymbol{\alpha}_{\mathcal{R}} \times \boldsymbol{u}) + 2(\boldsymbol{\omega}_{\mathcal{R}} \cdot \boldsymbol{u})\boldsymbol{u}' - (\boldsymbol{u} \times \boldsymbol{\omega}_{\mathcal{R}})(\boldsymbol{u} \cdot \boldsymbol{\omega}_{\mathcal{R}})$$

Introducing the libration angles (θ, φ) and performing some cumbersome algebraic work, these equations take the form

$$\theta'' - 2\varphi' \tan\varphi(\theta' + 1) + 3 \sin\theta \cos\theta = e[2h_1(\nu, e)(\theta' + 1) + 3h_2(\nu, e) \sin\theta \cos\theta] - \epsilon\{\tan\varphi \sin i[2g_1(e, \omega, \nu) \cos\theta - g_2(e, \omega, \nu) \sin\theta] + g_3(e, \nu) \cos i\} \tag{14}$$

$$\varphi'' + [(\theta' + 1)^2 + 3\cos^2\theta] \sin\varphi \cos\varphi = e[2h_1(\nu, e)\varphi' + 3h_2(\nu, e) \sin\varphi \cos\varphi \cos^2\theta] + \epsilon \sin i[2g_1(e, \omega, \nu) \sin\theta + g_2(e, \omega, \nu) \cos\theta] \tag{15}$$

where h_1, h_2, g_1, g_2, and g_3 are auxiliary functions given by

$$h_1(e, \nu) = \frac{\sin\nu}{1 + e\cos\nu}, \qquad h_2(e, \nu) = \frac{\cos\nu}{1 + e\cos\nu} \tag{16}$$

$$g_1(e, \omega, \nu) = \frac{\sin(\omega + \nu)}{1 + e\cos\nu}, \qquad g_2(e, \omega, \nu) = \frac{\cos(\omega + \nu)}{1 + e\cos\nu}$$

$$g_3(e, \nu) = \frac{1}{1 + e\cos\nu} \tag{17}$$

and the independent variable is the true anomaly ν measured from the perigee.

There are four free parameters in Eqs. (14) and (15): three orbital elements (e, i, ω) and the electrodynamic parameter ε, which is defined by

$$\varepsilon = (J_1/I_s)(\mu_m/\mu_E) \tag{18}$$

and gauges the electrodynamic torque vs the torque produced by the gravity gradient and inertia forces.

Obviously, Eqs. (14) and (15) must be integrated from the appropriate initial conditions:

$$\text{at} \quad \nu = \nu_0: \qquad \theta = \theta_0, \quad \varphi = \varphi_0, \quad \dot{\theta} = \dot{\theta}_0, \quad \dot{\varphi} = \dot{\varphi}_0 \tag{19}$$

corresponding to the instant in which the tether current is switched on.

Inert Tether

For an inert tether, that is, when no current flows in the wire, $\varepsilon = 0$, and the governing equations (14) and (15) reduce to

$$\theta'' - 2\varphi' \tan\varphi(\theta' + 1) + \tfrac{3}{2} \sin 2\theta = e\left[2h_1(\nu, e)\,(\theta' + 1) + \tfrac{3}{2} h_2(\nu, e) \sin 2\theta\right] \tag{20}$$

$$\varphi'' + [(\theta' + 1)^2 + 3\cos^2\theta]\tfrac{1}{2} \sin 2\varphi = e\left[2h_1(\nu, e)\varphi' + \tfrac{3}{2} h_2(\nu, e) \sin 2\varphi \cos^2\theta\right] \tag{21}$$

with h_1 and h_2 given by Eq. (16).

For a circular orbit, $e = 0$, the local vertical is a stable equilibrium position of Eqs. (20) and (21). In that position, the tether rotates uniformly about the orbit normal. However, for an elliptical orbit the local vertical does not rotate uniformly, and it is no longer an equilibrium position for the tether. In such cases, the tether librations become excited even if the tether is left at rest along the local vertical. The reason for this behavior is found in Eq. (20), which governs the oscillation of the in-plane angle and is a self-excited equation. Because of the coupling between the in-plane and the out-of-plane angles, the tether will oscillate continually, and these oscillations grow with the eccentricity e. Instead of equilibrium positions along the local vertical, the governing equations have periodic solutions that play an important role because the dynamic stability of the system is given by their stability properties.

The problem that we face here has been considered long ago in the literature from different points of view. For instance, the libration of gravity-gradient satellites exhibits a self-excited dynamics that is

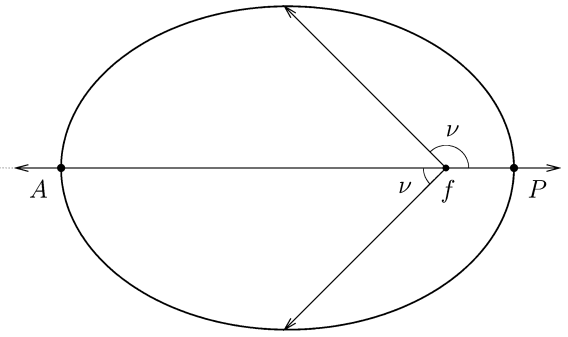

Fig. 3 Eccentricity ranges in [0,1].

strongly chaotic in some regions of the parameter space.[9] With no intention to be comprehensive, we give some references where this problem has been discussed.[6,7,9–15] Regarding the aim of this paper, the central references are Refs. 6 and 7, where Modi and Brereton, in 1969, found different families of periodic solutions for the more general problem of a satellite in elliptical orbit. In their analysis, the tethered satellite turns out to be a particular case. They studied the in-plane oscillation, because Eq. (21), which is not self-excited, provides the solution $\varphi(\nu) \equiv 0$ for the initial conditions $\varphi_0 = \dot{\varphi}_0 = 0$. Thus, without any other perturbation the periodic solutions appearing in elliptical orbits correspond to in-plane oscillations, and they are governed by the equation

$$\theta'' + 3\sin\theta\cos\theta = e[2h_1(\nu, e)(\theta' + 1) + 3h_2(\nu, e)\sin\theta\cos\theta] \tag{22}$$

The first task to carry out is to reproduce the results of Refs. 6 and 7, which will be taken as the starting point of the analysis developed in this paper. However, we take a quite different approach closely related with the numerical tool used to obtain families of periodic orbits. We work with a slightly modified version of the numeric algorithm developed in Ref. 8, which is based on the Poincaré method on the analytical continuation of periodic orbits.[16] The algorithm provides the stability properties of the periodic orbits after having detected them.

The first step in using the algorithm is to rewrite the governing equations as a forced system. Equations (20–22) have been rewritten in this way. On their left-hand sides, we find the terms corresponding to the circular case equations, and on the right-hand sides the perturbation that the eccentricity introduces into the system. Note that such a perturbation is described through periodic forcing terms whose period coincides with the orbital period.

In Refs. 6 and 7 the eccentricity ranges in the interval $[-1, 1]$. In this paper, however, the eccentricity ranges in the interval $[0, 1]$. A negative eccentricity means that the true anomaly ν is measured from the apogee, that is, it has been shifted in π (Fig. 3). We always measure the true anomaly ν from the perigee, and therefore $e \in [0, 1]$.

We use the numeric algorithm as follows: starting from a periodic orbit corresponding to the circular case ($e = 0$), we propagate the family of periodic orbits for increasing values of e. Thus, we need a periodic orbit of the circular case from which to start the propagation.

Because of the frequency entrainment law,[17] the periodic solutions appearing in the elliptical case must have the orbital period, or an integer multiple of it. Therefore, we can select for the circular case $e = 0$, the appropriate periodic orbit from which the propagation process will start. As a consequence, we begin the analysis summarizing the main aspects of the circular case.

Circular Case

For the circular case, Eq. (22) becomes

$$\theta'' + 3\sin\theta\cos\theta = 0 \tag{23}$$

and it has the energy integral

$$(\theta')^2 + 3\sin^2\theta = 3\sin^2\theta_M$$

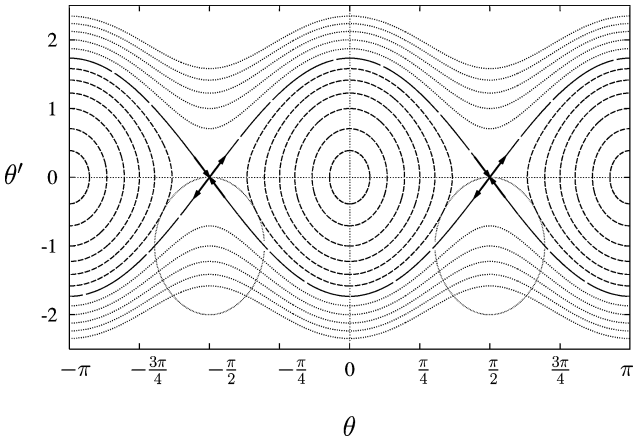

Fig. 4 Phase plane of the gravity-gradient pendulum.

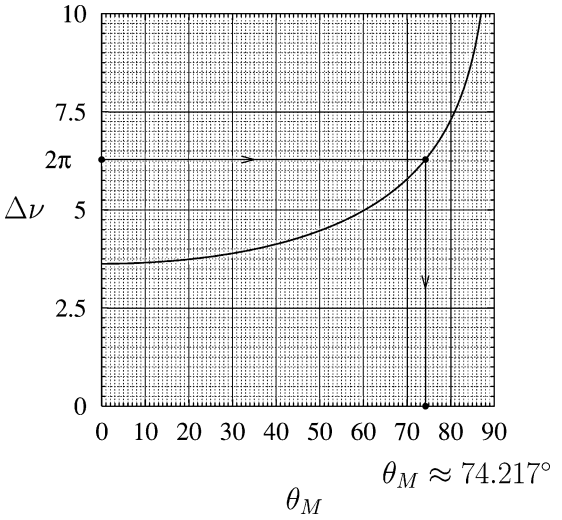

Fig. 5 $\Delta\nu$ in a libration cycle.

where the amplitude θ_M is given by the initial conditions

$$\nu = \nu_0: \qquad \theta = \theta_0 = 0, \quad \theta' = \theta'_0 = \sqrt{3}\sin\theta_M$$

Note that θ_M and θ'_M are equivalent data, and any of the two variables can be used to describe the initial condition of a phase plane periodic orbit. Figure 4 shows the orbits in the phase space. When $\theta_M < 90$ deg, the motion is a libration and when $\theta_M > 90$ deg, a rotation. For $\theta_M = 90$ deg, we have equilibrium positions and separatrices that correspond to asymptotic motions separating the libration from the rotation. We are interested in librations that in the circular case are always associated with periodic motion.

A new integration provides the solution

$$\sin\theta = \sin\theta_M \cdot \mathrm{sn}\left[\sqrt{3}(\nu - \nu_0), \sin\theta_M\right] \tag{24}$$

where $\mathrm{sn}(u, \sin\theta_M)$ is the Jacobian elliptic function with modulus $m = \sin^2\theta_M$.

The function $\mathrm{sn}(u, \sin\theta_M)$ is periodic in u. Its period is $4K(\theta_M)$, where $K(\theta_M)$ is the complete elliptic integral of the first kind:

$$K(\sin\theta_M) = \int_0^{\pi/2} \frac{\mathrm{d}\zeta}{\sqrt{1 - \sin^2\theta_M \sin^2\zeta}}$$

Therefore, during a whole libration cycle the increase of the true anomaly is given by

$$\Delta\nu = \left(4/\sqrt{3}\right)K(\sin\theta_M) \tag{25}$$

and it is plotted in Fig. 5 as a function of θ_M. Notice that the function $\Delta\nu = \Delta\nu(\theta_M)$ increases monotonously from is minimum value $\Delta\nu(0) = 2\pi/\sqrt{3} \approx 3.63$ at $\theta_M = 0$ until $\Delta\nu(90) = \infty$ at $\theta_M = \pi/2$.

Table 1 Periodic solutions

$m\backslash n$	1	2	3	4	5
1	2π	4π	6π	8π	——
2	π	2π	3π	4π	——
3	$2\pi/3$	$4\pi/3$	2π	$8\pi/3$	——
4	$\pi/2$	π	$3\pi/2$	2π	——
5	$2\pi/5$	$4\pi/5$	$6\pi/5$	$8\pi/5$	——
6	——	——	——	——	——

The solutions for which $\Delta\nu = 2\pi n/m$ (m and n integers) are particularly interesting. They correspond to situations in which the tether completes m whole libration cycles while the center of mass G describes n orbits.

When $n = 1$, there is only one such solution. It corresponds to $m = 1$, when $\Delta\nu(\theta_M) = 2\pi$. [Note that $m = 2$ yields $\Delta\nu = \pi$, which is lower than $\Delta\nu(0) \approx 3.63$, and therefore there is no solution.] The procedure giving the solution is shown in Fig. 5, and it provides $\sin\theta_M \approx 0.9623$. The corresponding initial conditions are $\theta_M \approx 74.217$ deg (or $\theta_0' \approx \pm 1.667$).

These initial conditions lead to a pair of 2π-periodic orbits: 1) for the first one, which will be named $\mathcal{P}_1$, we have $\theta_0' \approx +1.667$; and 2) the second one, which will be named $\mathcal{P}_2$, we have $\theta_0' \approx -1.667$. Both orbits are identical and describe the same trajectory in the phase plane (θ, θ'). However, they are 180 deg out of phase. We anticipate a rather different behavior for $e \neq 0$.

At first sight, when $n = 2$ there are three possibilities: $m = 1$, 2, and 3. Obviously, the case $m = 2$ coincides with the case just considered, and it will be discarded. We have two 4π-periodic solutions for each one of the cases $m = 1$ and $m = 3$. Thus, the following is noted:

1) If $m = 3$, the increase will be $\Delta\nu(\theta_{M_2}) = 4\pi/3$ and will lead to $\sin\theta_{M_2} \approx 0.67074$, $\theta_{M_2} \approx 42.12404$ deg, and $\theta_2'(0) \approx \pm 1.16175$. The orbits will be named $\mathcal{P}_{3a}$ [upper sign (+)] and $\mathcal{P}_{3b}$ [lower sign (−)].

2) If $m = 1$, the increase will be $\Delta\nu(\theta_{M_1}) = 4\pi$ and will lead to $\sin\theta_{M_1} \approx 0.99985$, $\theta_{M_1} \approx 89.00647$ deg, and $\theta_1'(0) \approx \pm 1.73179$. The orbits will be named $\mathcal{P}_{4a}$ [upper sign (+)] and $\mathcal{P}_{4b}$ [lower sign (−)].

When $n = 3$, there are four possibilities: $m = 1$, $m = 2$, $m = 4$, and $m = 5$. All of them lead to 6π-periodic solutions. Using this procedure, we would fill in Table 1 and obtain periodic solutions of increasing period in a systematic way. However, we will only consider the cases $n = 1$ and $n = 2$ for reasons that will be revealed later on.

There are also equilibrium positions for which $\theta = \theta' = 0$, with the tether aligned along the local vertical and at rest. These steady solutions could also be considered as periodic solutions. In such a case, the period can be selected freely.

Each one of the periodic solutions that have been obtained in this way belongs to a wider family of periodic solutions. The eccentricity e is the parameter of such a family.

Families of Periodic Orbits for the Elliptic Case

We begin the analysis showing the families of periodic orbits that oscillate with the orbital period, 2π in nondimensional form.

2π-Periodic Orbits

Figure 6 shows three families of periodic solutions that have been obtained in our analysis. The upper picture shows their phase plane trajectories, the lower one their time history in one orbital period. In both cases, three values of the eccentricity e have been considered: $e = 0.1$, 0.2, and 0.3. The arrows show the direction of the families for increasing values of e.

Note that for all of the periodic solutions found, the tether crosses the local vertical at the apogee and the perigee. Moreover, it does not reach the maximum amplitude on the intermediate points $(\nu = \pi/2;\ \nu = 3\pi/2)$.

The family labeled $\mathcal{F}_1$ is the continuation, for values of $e \neq 0$, of the periodic orbit named $\mathcal{P}_1$ in the preceding analysis. For this orbit, the initial value θ_0' is positive, and the amplitude of the oscillation decreases when e increases.

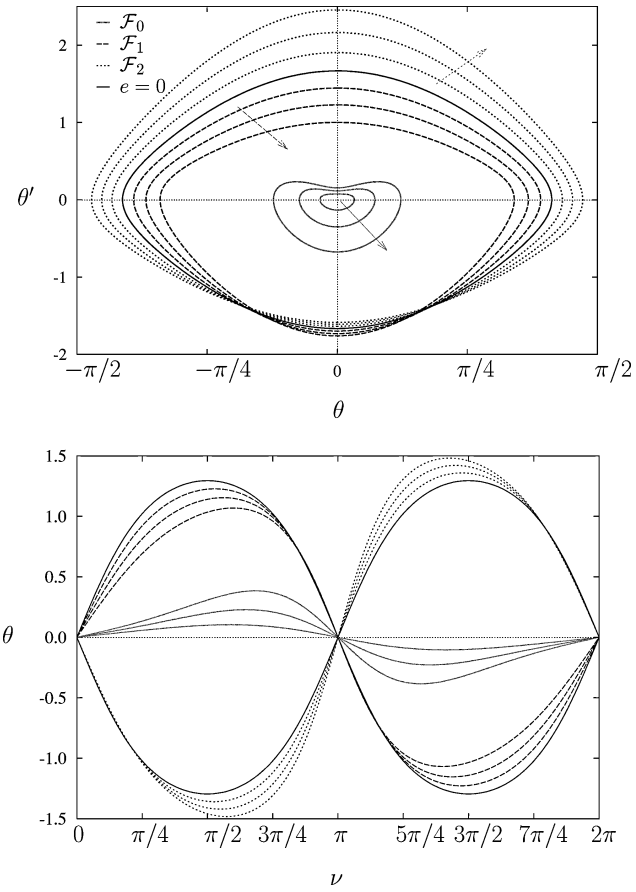

Fig. 6 Three families of 2π-periodic orbits for increasing values of e: 0.1, 0.2, and 0.3.

The family labeled $\mathcal{F}_2$ is the continuation, for values of $e \neq 0$, of the periodic orbit named $\mathcal{P}_2$ in the preceding analysis. For this orbit, the initial value θ_0' is negative, and the amplitude of the oscillation increases when e increases.

The orbits $\mathcal{P}_1$ and $\mathcal{P}_2$ appear in Fig. 6 as the trajectory labeled $e = 0$, and they share the same phase plane trajectory. However, they have different time histories, which exhibit a phase lag of one semiperiod.

Note that the phase flow of Eq. (23) does not depend on the sign of θ'. However, Eq. (14) does not have such a property, and a change of sign in θ' leads to a quite different orbit in the phase plane. This is the reason why, from the same periodic orbit of the phase plane, two different families arise for $e \neq 0$.

The family labeled $\mathcal{F}_0$ arises from the stable equilibrium position $(\theta = \theta' = 0)$. For this family, θ_0' is positive, and the amplitude of the oscillation increases when e increases. Because the oscillation goes to zero with e, it is possible to obtain an asymptotic approximation for these orbits in the limit $e \to 0$. Such an approximation is given by Eq. (26):

$$\theta(\nu, e) = \sin\nu \cdot e - \tfrac{3}{2}\sin 2\nu \cdot e^2 + \left[(13/12)\sin 3\nu + \tfrac{3}{4}\sin\nu\right] \cdot e^3 + \left[\tfrac{7}{4}\sin 2\nu - (83/104)\sin 4\nu\right] \cdot e^4 + \mathcal{O}(e^5) \tag{26}$$

Figure 7 shows the asymptotic solution, plotted with solid lines, and the solution obtained numerically plotted with dots. Both solutions show a good agreement for the three values of e considered: 0.1, 0.2, and 0.3. Obviously, the agreement is better for the smallest values of e. If necessary, it would be possible to increase the accuracy of the asymptotic solution (26) obtaining more terms of the expansion. The procedure is explained in detail in Refs. 1 and 2.

Each orbit is determined by the initial conditions $\theta_0 = 0$ and θ_0'. To obtain a periodic solution in a particular case, only the value of θ_0' is needed because the integration of the governing equation in one period provides the time history of that particular solution. Figure 8

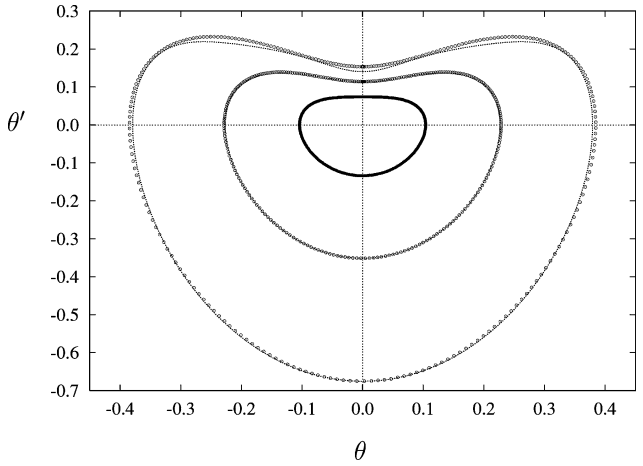

Fig. 7 Asymptotic solution (26) (——) and the numeric one for the family $\mathcal{F}_0$ ($e = 0.1$, 0.2, and 0.3).

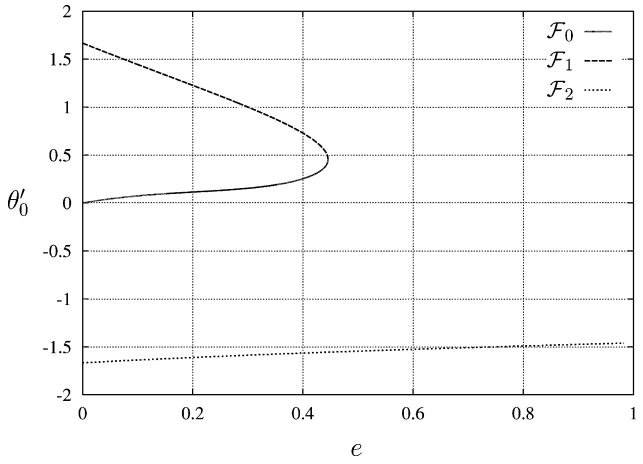

Fig. 8 Initial conditions vs e for the families $\mathcal{F}_0$, $\mathcal{F}_1$, and $\mathcal{F}_2$.

shows the initial conditions corresponding to the three families $\mathcal{F}_0$, $\mathcal{F}_1$, and $\mathcal{F}_2$ vs the eccentricity e.

The families $\mathcal{F}_0$ and $\mathcal{F}_1$ merge for the value $e \approx 0.446$ (point C in Fig. 9). For larger values of e, both families disappear. The family $\mathcal{F}_2$, on the other hand, does not disappear, and it exists even for values of e close to unity. However, its numeric determination becomes involved when e approaches unity because of Eq. (14), which is singular for $e = 1$.

For the family $\mathcal{F}_0$, the monodromy matrix of the periodic solution has two eigenvalues. Figure 9 shows, in the upper picture, these eigenvalues as a function of the eccentricity e. The lower picture shows their moduli vs e. The modulus of one eigenvalue is greater than unity in the interval $I_0 \approx [0.3533, 0.4273]$ ($I_0 \equiv [A, B]$ in Fig. 9), where the family is unstable. Outside I_0 the family is linearly stable. At the boundary values of I_0 (points A and B in Fig. 9), both eigenvalues take the value $\lambda = -1$. This situation is typical of flip bifurcations, in which the period of the solution will be doubled. A more detailed analysis about this matter can be found in Ref. 9. Note that a classical path to chaotic motion can be found in a cascade of consecutive flip bifurcations. An interesting analysis on the control of chaotic motion in the problem discussed here can be found in Ref. 9.

From the point of view of the operation of an electrodynamic tether, only the family $\mathcal{F}_0$ is interesting. The other two families, $\mathcal{F}_1$ and $\mathcal{F}_2$, turn out to be very unstable. Figure 10 shows the moduli of the eigenvalues of the monodromy matrix for these two families. The upper picture corresponds to the $\mathcal{F}_1$ family, which ends in $e \approx 0.446$, where it merges with family $\mathcal{F}_0$. The modulus of the unstable eigenvalue reaches values of the order of 20. The lower picture corresponds to the $\mathcal{F}_2$ family, which exists practically

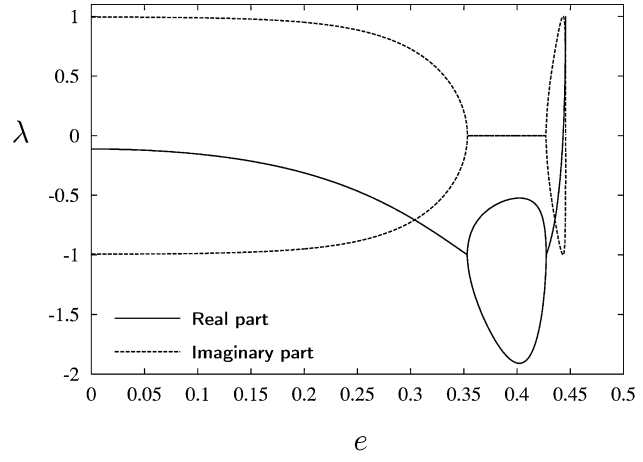

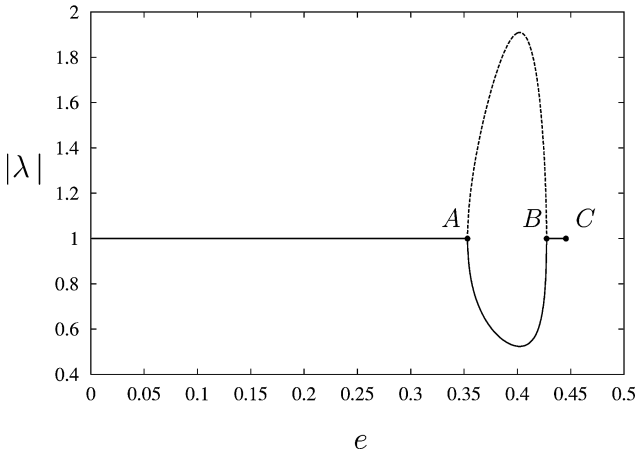

Fig. 9 Eigenvalues of the monodromy matrix and moduli for the family $\mathcal{F}_0$.

over the entire range $e \in [0, 1]$. It is linearly stable in a very short interval $\approx [0, 0.046]$ close to the circular orbit. Beyond this interval, the modulus of the unstable eigenvalue increases monotonously until it reaches huge values (of the order of 10,000) when e is close to unity.

Out-of-Plane Perturbations

The analysis carried out in the preceding subsection is based on Eq. (22), and it does not take into account the effects of the out-of-plane perturbations. In our numeric scheme, it is easy to introduce these effects by simply adding Eq. (21) to the analysis. Thus, it is necessary to repeat the analysis replacing Eq. (22) by the system (20) and (21).

Because of the strongly unstable character of the families $\mathcal{F}_1$ and $\mathcal{F}_2$, the new analysis including the out-of-plane perturbations has been carried out only for the $\mathcal{F}_0$ family. The main novelty lies in a new eigenvalue of the monodromy matrix associated to the new degree of freedom. Figure 11 shows the modulus of the eigenvalues of the monodromy matrix, including the new eigenvalue, as a function of e.

Note that in the interval $\approx [0, 0.3533]$, where the periodic solutions were linearly stable when subjected only to in-plane perturbations, the family now becomes unstable. As a result, the family $\mathcal{F}_0$ is stable only in the short interval $e \in [0.4273, 0.4456]$. However, for small values of e ($e < 0.2$ approximately) the instability is very weak.

4π-Periodic Orbits

Two families have been found whose period is twice the orbital period. For the first family, which we will name $\mathcal{F}_3$, the tether completes three libration cycles in two orbits ($m = 3$). For the second family, which will be named $\mathcal{F}_4$, the tether only completes one

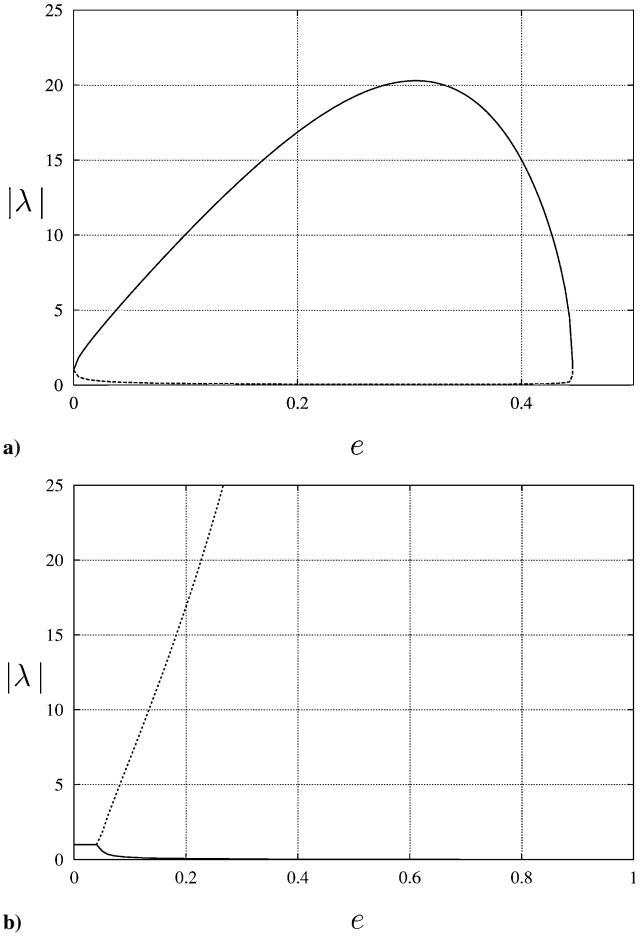

Fig. 10 Moduli of the eigenvalues of the monodromy matrix. Families a) $\mathcal{F}_1$ and b) $\mathcal{F}_2$.

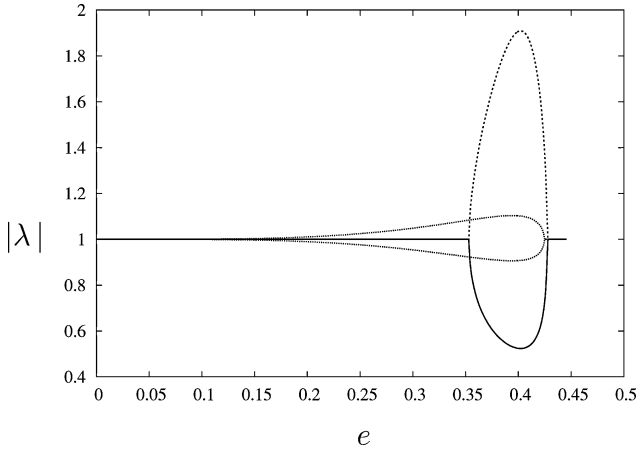

Fig. 11 Moduli of the eigenvalue for the $\mathcal{F}_0$ family.

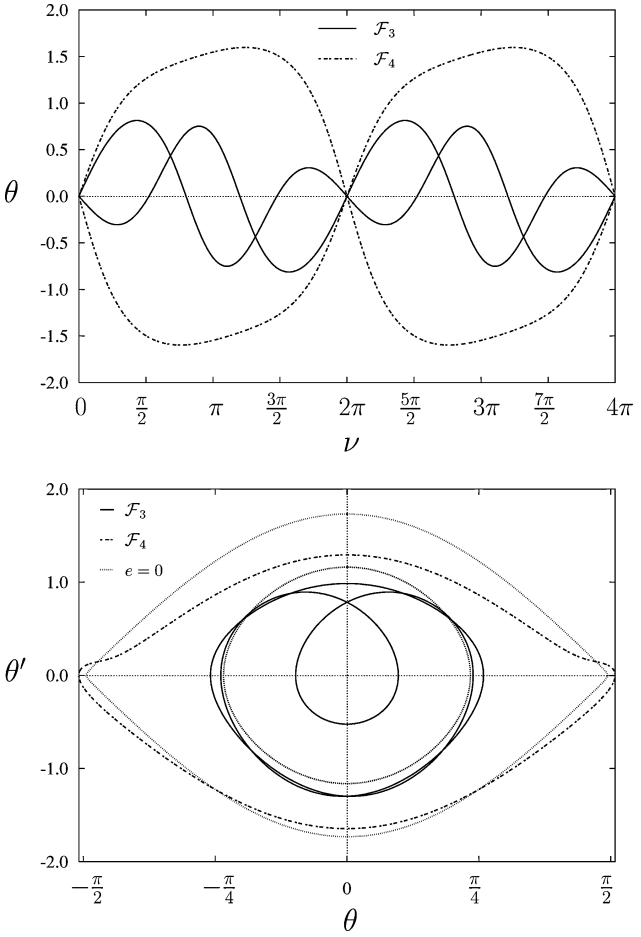

Fig. 12 Periodic solutions of families $\mathcal{F}_3$ and $\mathcal{F}_4$ for $e=0.2$.

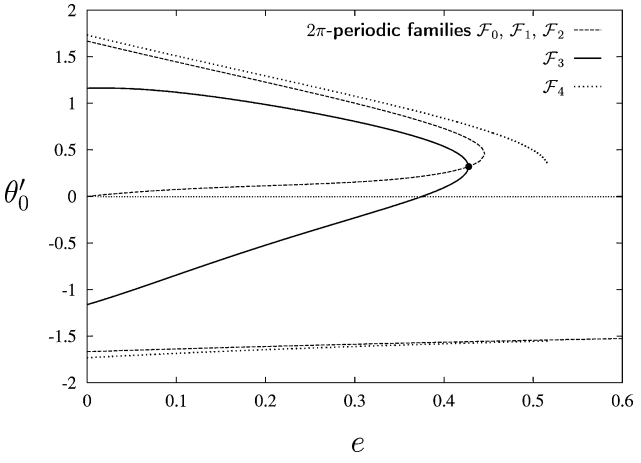

Fig. 13 Initial conditions for the families $\mathcal{F}_3$ and $\mathcal{F}_4$ vs e.

libration cycle ($m=1$). Figure 12 shows, in its upper picture, the time history, over two orbital periods, of some periodic orbits of these families, when the eccentricity is $e=0.2$. The lower picture of this figure shows the trajectories of these periodic orbits in the phase plane.

The family $\mathcal{F}_3$, for example, has two subfamilies: one which is the continuation for values of $e\neq 0$ of the periodic orbit $\mathcal{P}_{3a}$ of the circular case; for this periodic orbit, $\theta_0'>0$. The other subfamily is the continuation for values of $e\neq 0$ of the periodic orbit $\mathcal{P}_{3b}$ of the circular case; for this periodic orbit, $\theta_0'<0$. Both subfamilies are one orbital period phased out, and they share the same trajectories in the phase plane. Figure 12 shows, in its lower picture, the trajectory corresponding to the circular case (orbits $\mathcal{P}_{3a}$ and $\mathcal{P}_{3b}$) and the trajectory shared by the two periodic orbits of the family $\mathcal{F}_3$ plotted in the upper picture.

A similar situation holds for the family $\mathcal{F}_4$. It also contains two subfamilies, which are the continuation for values of $e\neq 0$ of the periodic orbits $\mathcal{P}_{4a}$ and $\mathcal{P}_{4b}$ of the circular case. Figure 12 shows the corresponding curves for this family.

Figure 13 shows the initial conditions corresponding to the 4π-periodic families $\mathcal{F}_3$ and $\mathcal{F}_4$ and the 2π-periodic families $\mathcal{F}_0$, $\mathcal{F}_1$, and $\mathcal{F}_2$. The two subfamilies of the $\mathcal{F}_3$ family, which for $e=0$ start in opposite points, merge for the values ($e\approx 0.4273$, $\theta_0'\approx 0.32$). In this particular point, a flip bifurcation takes place, and two orbits of double period bifurcate from the 2π-periodic orbit. The two

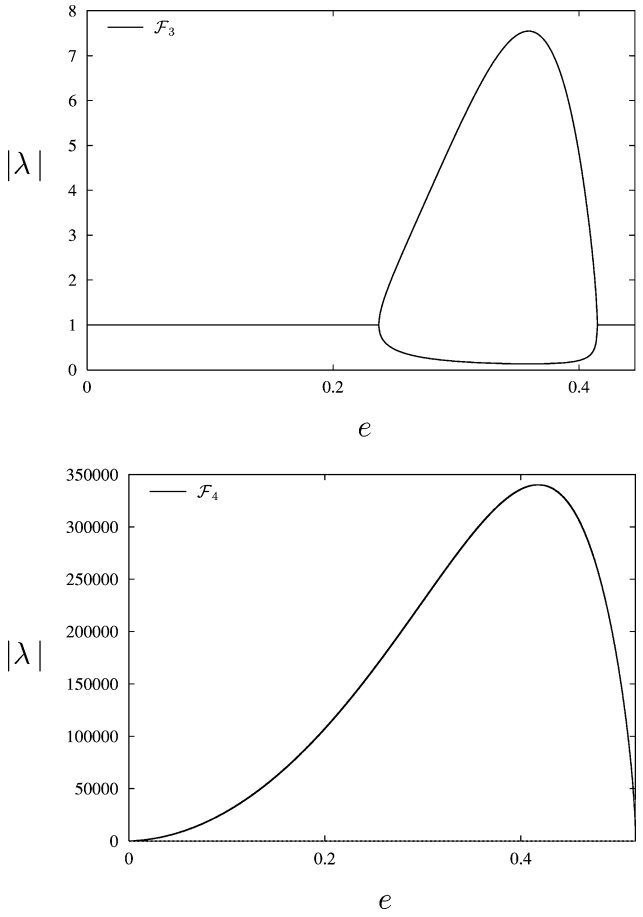

Fig. 14 Moduli of the eigenvalues for the families $\mathcal{F}_3$ and $\mathcal{F}_4$ vs e.

subfamilies of the $\mathcal{F}_4$ family, which also start in opposite points for $e = 0$, never merge. Both subfamilies end when e reaches the value $e \approx 0.51556$.

Figure 14 shows the moduli of the eigenvalues of the monodromy matrix for the two families $\mathcal{F}_3$ and $\mathcal{F}_4$. The family $\mathcal{F}_3$ is linearly stable in the intervals [0, 0.237] and [0.415, 0.4456] and very unstable in the interval [0.237, 0.415]. The out-of-plane perturbations do not modify this behavior. Because of its high instability, the interest of family $\mathcal{F}_3$ is small. However, it could be taken as the starting point for the operation of the electrodynamic tether because in the interval [0, 0.237] it is more stable than the 2π-periodic family $\mathcal{F}_0$.

The family $\mathcal{F}_4$ is strongly unstable. Because each family has two subfamilies, Fig. 14 should contain four pictures (one for each subfamily). However, for each family both subfamilies share the same eigenvalues. This numeric result has been confirmed and checked thoroughly for the $\mathcal{F}_3$ family. The calculations for the $\mathcal{F}_4$ family, because of its huge instability, are rather involved, and they have not been checked because the interest of this family is slender, from the point of view of the operation of the electrodynamic tether.

It should be possible to follow the analysis studying the periodic families with periods 6π, 8π, ... and so on. However, all of those families, as in the case of the preceding family $\mathcal{F}_4$, are not interesting for space tethers, at first sight. Their analysis is not included in this paper.

Alive Tether

When the tether is alive, that is, when the current is flowing in the wire, the parameter $\varepsilon \neq 0$. In such a case, there are four free parameters in the problem: e, ε, i, and ω.

To show the influence of the eccentricity, we will start from the circular case ($e = 0$), whose analysis has been carried out in Ref. 3. Notice that for $e = 0$, the number of free parameters becomes two because the argument of the perigee ω disappears. In this case, for each pair of values of the free parameters (ε, i) there is a basic 2π-periodic solution that can be determined.

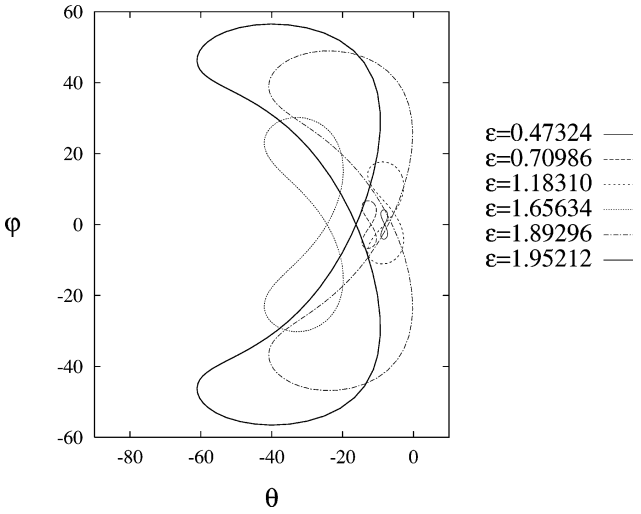

Fig. 15 Periodic solution of the circular case for $i = 25$ deg and different values of ε.

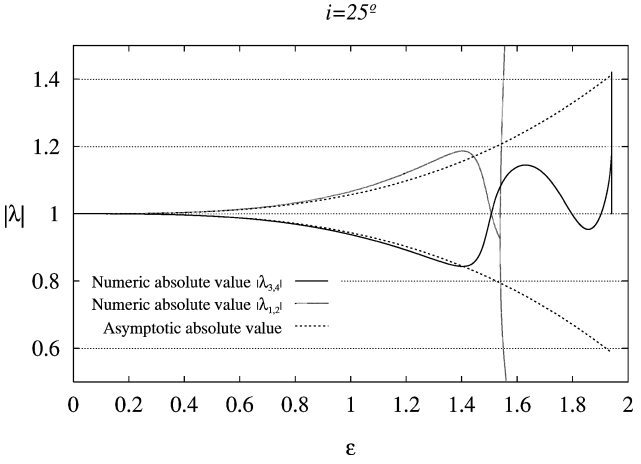

Fig. 16 Moduli of the eigenvalues of the monodromy matrix for $e = 0$. The inclination is $i = 25$ deg.

Figure 15 shows some of these periodic solutions when $i = 25$ deg and for different values of ε. (Figures 15–17 have been taken from Ref. 3.) Each one of these basic periodic solutions belongs to a wider family of 2π-periodic solutions, which can be continued for nonvanishing values of e. For given values of (ε, i), this family can be propagated, starting from the circular case, by increasing the values of e. This way, the influence of a nonvanishing eccentricity in the problem will be described. This is the main goal of this work.

To increase the legibility of the paper, we will summarize concisely the more important points of the circular case studied in Ref. 3. In most of the cases, the monodromy matrix has four eigenvalues that appear as two pairs of complex conjugate numbers. Figure 16, in which the inclination is $i = 25$ deg, shows the moduli of the eigenvalues of the monodromy matrix as a function of ε (circular case). You can see in the figure a special value of ε, close to 1.5, for which the moduli of all eigenvalues become 1. Just behind this value, one pair of complex conjugate eigenvalues splits up into two real numbers when ε reaches a critical value ε^*, which is a function of i. (It is close to $\varepsilon^* \simeq 1.54$ when $i = 25$ deg in Fig. 16.) Figure 17 depicts this function $\varepsilon = \varepsilon^*(i)$, which divides the plane (i, ε) in two regions. In one of them, the instability is weak, and the control of the electrodynamic tether would be easier. We remember that the instability considered in these pages appears when dissipation, or damping, is not considered in the system. By introducing dissipation,

or some kind of control, the system would become stable in some cases.[18,19]

The first thing to be underlined is the change of the shape of the periodic solution when both effects, electrodynamic forces and eccentricity, act on the tether.

Figure 18 shows the shape of the periodic solution for two inclinations and two values of the argument of the perigee. The upper pictures correspond to $i = 25$ deg, $\omega = 30$ deg, and the lower ones to $i = 45$ deg, $\omega = 0$ deg. In the left pictures, $\varepsilon = 0.5$, and the eccentricity take the values $e = 0.001$, 0.01, 0.05, 0.1, 0.2, and 0.3. In the right pictures, $\varepsilon = 0.75$, and the eccentricity take the values $e = 0.001$, 0.01, 0.05, 0.1, 0.2, and 0.28. In all cases, for small values of e the periodic solution has the shape of an eight, and it is quite similar to the curves shown in Fig. 15 for the circular case. However, for increasing values of e the shape changes very fast and ends up turning into something similar to an inverted U. Because of the self-excited character of the equation for the in-plane angle, the oscillation in θ probably becomes more pronounced that the out-of-plane oscillation.

The more important issue to be considered in this analysis is the stability properties of these 2π-periodic solutions. In particular, we are interested in the evolution of these stability properties, when e takes increasing values starting from $e = 0$. For the elliptic case, the four eigenvalues of the monodromy matrix appear as two pairs of complex conjugate numbers.

Figure 19 shows the moduli of these eigenvalues as a function of the eccentricity e for the particular case $\varepsilon = 0.5$, $i = 25$ deg, and $\omega = 30$ deg. This case has been selected because it shows very well

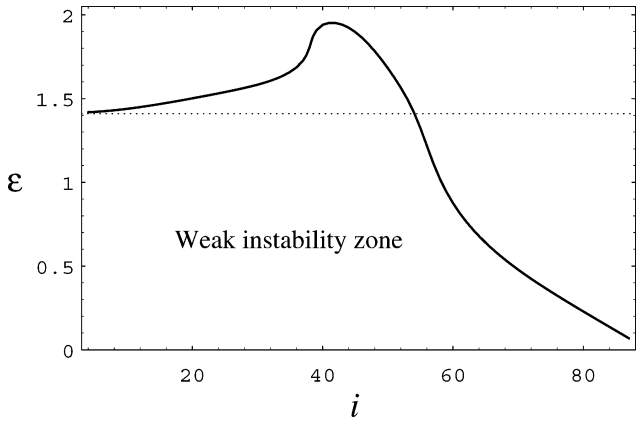

Fig. 17 Regions of weak and strong instability in the plane (i, ε) for the circular case.

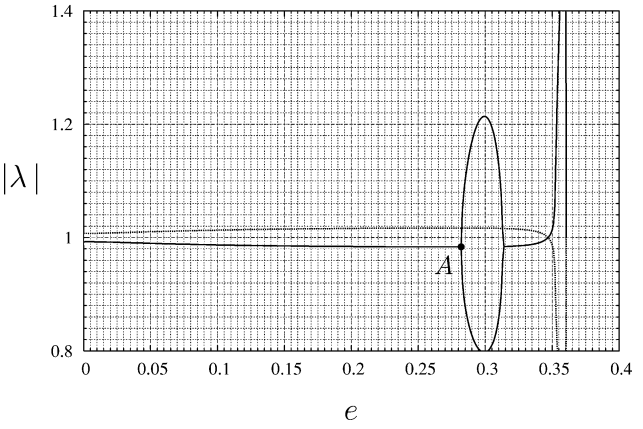

Fig. 19 Moduli of the eigenvalues of the monodromy matrix vs e for $\varepsilon = 0.5$, $i = 25$ deg, and $\omega = 30$ deg.

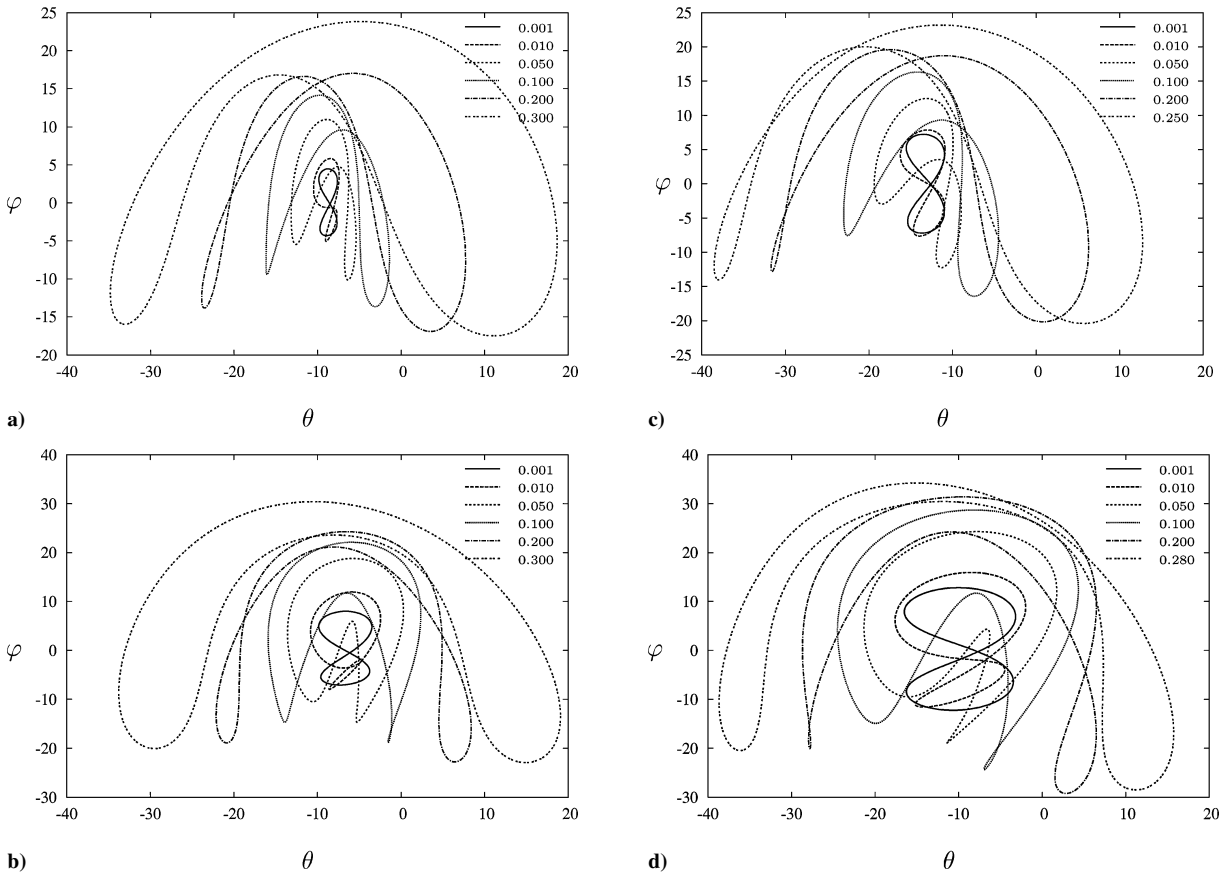

Fig. 18 Form of the basic periodic solution for a) and b) $\varepsilon = 0.5$ and c) and d) $\varepsilon = 0.75$. a) and c) $i = 25$ deg, $\omega = 30$ deg and b) and d) $i = 45$ deg, $\omega = 0$ deg. Different values of e have been considered.

the essential qualitative behavior of the system. Different values of (ε, i, ω) provide quantitative changes, but the qualitative variations are not important.

In Fig. 19, the starting point $e = 0$ provides the moduli of the eigenvalues for the circular case, which we take as the reference values. For small values of e, the moduli of the eigenvalues do not change significantly, and for increasing values of e this situation remains unchanged until the point A in Fig. 19 is reached. This point corresponds to e^*, a critical value of the eccentricity for which one pair of conjugate complex eigenvalues splits into two real numbers and one of them grows significantly and abruptly. In Fig. 19, $e^* \approx 0.283$. Thus, for values of $e < e^*$ the instability associated to the electrodynamic forces remains almost the same as in the circular orbit, but for $e > e^*$ the instability becomes more pronounced. As a consequence, the critical value e^* will be useful to separate the cases of weak instability from the cases of strong instability.

In this analysis, the critical value e^* is a function of the other free parameters: $e^* = e^*(\varepsilon, i, \omega)$. The effect of all of these parameters will be plotted in the (e, ε) plane. For given values of i and ω, the critical condition defines a curve in the plane (e, ε). Such a curve divides the plane in two regions: in one of them the instability is weak, as in the circular case, but in the other one, the instability becomes strong. In the region of weak instability, the control of the electrodynamic tether would be easier.

To study the effect of both parameters (i and ω), first ω will be kept fixed and equal to zero, studying in this way the effect of changing the value of i. In a second step the effect of ω will be studied. Figure 20 shows the curves $e^* = e^*(\varepsilon, i, 0)$ for the following values of the inclination: $i = 5$, 10, 20, 25, 30, and 35 deg. Note that in Fig. 20, the curves for the different inclinations considered are close to each other. This means that the influence of the inclination is small.

For small values of e, the critical value e^* does not separate the weak instability zone of the strong instability zone very well. The reason must be found in the behavior of the eigenvalues for increasing values of ε. When ε increases, Fig. 19 changes in the following way: 1) the point A moves to the left, and 2) the central oval shrinks. Figure 21 shows the moduli of the eigenvalues for $\varepsilon = 0.9$, and the same inclination and argument of perigee $i = 25$ deg, $\omega = 30$ deg. It is clear that just beyond the point A of the figure the eigenvalues do not have large moduli. In these cases it is better to use the point B of this figure. In B, the modulus of all of the complex eigenvalues is unity. However, beyond B the moduli of one pair of conjugate complex eigenvalues grow very quickly, and this means strong instability. Thus, in those cases the weak and the strong instability zones are better separated using the point B.

Figure 20 also shows the curves described by the point B in the plane (e, ε) for the same values of the inclination. These new curves again exhibit a low sensitivity to the inclination. Roughly speaking,

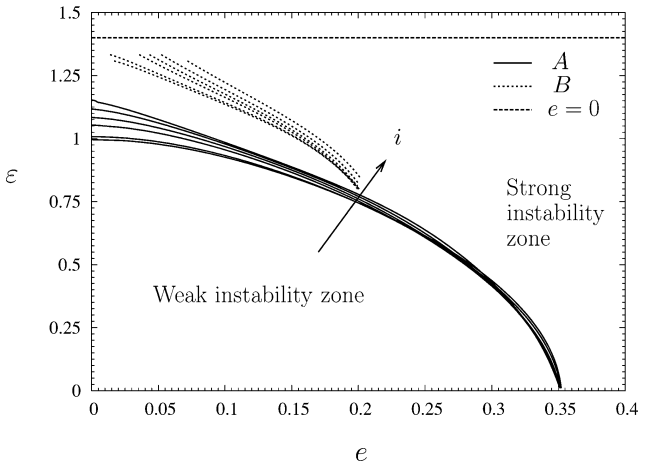

Fig. 20 Regions of the plane (e, ε) with different stability properties.

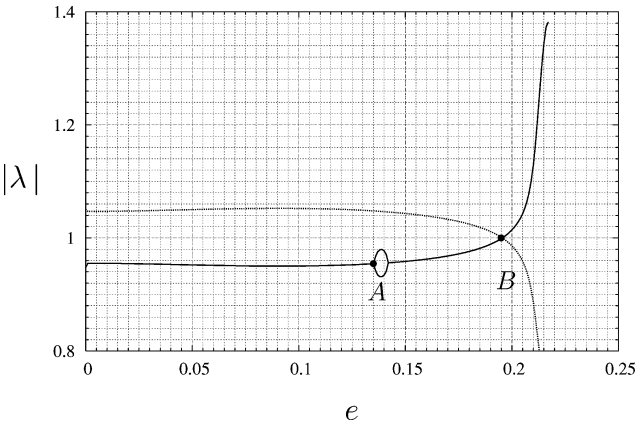

Fig. 21 Moduli of the eigenvalues of the monodromy matrix vs e for $\varepsilon = 0.9$, $i = 25$ deg, and $\omega = 30$ deg.

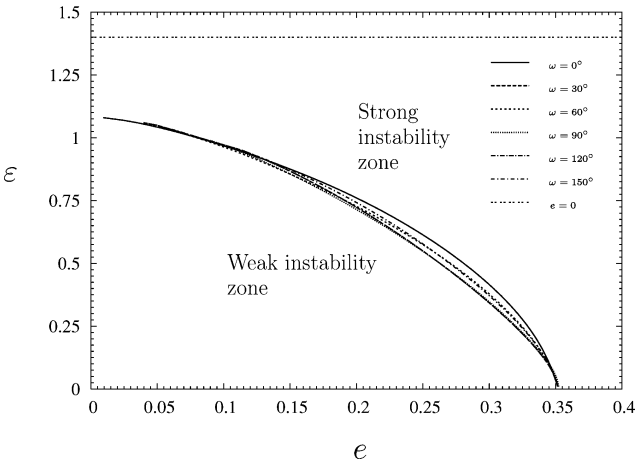

Fig. 22 Regions of the plane (e, ε) with different values of ω.

for $e > \approx 0.2$ the separation between the weak and strong instability zones is well described by the A curves, but for $e < \approx 0.2$ is better to use the B curves.

The upper horizontal line in Fig. 20 corresponds to the circular case. It gives the order of magnitude of the critical value of ε (see Fig. 17), which separates the weak from the strong instability zone in the circular orbit.

Now in a second step, the effect of ω is studied, keeping the inclination fixed to $i = 25$ deg. Figure 22 shows the different curves $e^* = e^*(\varepsilon, 25, \omega)$ for the following values of the argument of the perigee ω: $\omega = 0$, 30, 60, 90, 120, and 150 deg.

Only values of ω between 0 and 180 deg are considered. The reason for that can be found in Eqs. (14) and (15). They remain invariant under the transformation $\omega \to \omega + 180$ deg, $\theta \to \theta$, $\varphi \to -\varphi$. This means that orbits where the apogee and the perigee are shifted exhibit symmetric trajectories with respect to φ in the phase space, not in the real space. In Fig. 23 two periodic solutions are depicted, for $e = 0.2$, $\varepsilon = 0.5$, $i = 45$ deg, $\omega_1 = 30$ deg, and $\omega_2 = 210$ deg, respectively. These two trajectories have the same eigenvalues and of course stability properties, thus only the interval $\omega \in [0\ \ 180$ deg] needs to be studied. This symmetry appears to be caused by the simplifications assumed for the model.

From Fig. 22, one can conclude that the effect of ω is also small considered with the effect of the eccentricity, which can be considered as the driving parameter to study the stability of the problem. In any case, as expected, when $\varepsilon \to 0$ and also when $e \to 0$ the effect of the argument of the perigee is negligible. In the first case, the reason is that when the magnetic forces vanished ω disappears from Eqs. (14) and (15) as it has no influence on the gravitational forces.

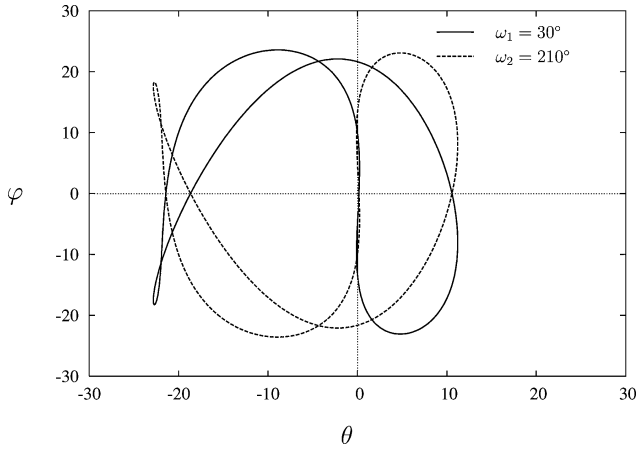

Fig. 23 Two trajectories of the tether in the phase space: $e = 0.2$, $\varepsilon = 0.5$, $i = 45$ deg, $\omega_1 = 30$ deg, and $\omega_2 = 210$ deg, respectively.

In the second case, when $e \to 0$ the orbit becomes circular, and ω is not defined for this case.

Figure 22 only shows the critical A curves (obtained with the help of point A). A similar analysis can be done by using the B point to separate, in the plane (e, ε), the weak instability zone from the strong one. However, because of the small sensitivity of the problem with the argument of the perigee ω the B curves do not change substantially from the curves shown in Fig. 20.

An important result emerging from this analysis is that, globally, the weak instability zone shrinks when the orbit is elliptical. Moreover, when the eccentricity is greater than ≈ 0.35 the electrodynamic tether becomes strongly unstable. This is particularly interesting because in some missions to the giant planets electrodynamic tethers have been considered as the primary power source in combination with elliptical orbits. In those cases, the eccentricity of the orbit must be lower than the critical value 0.35, to avoid the strong instabilities shown in this paper.

Conclusions

In this paper we study the effects of the joint action of the orbital eccentricity and electrodynamic forces on the attitude dynamics of an electrodynamic tether. For an elliptical orbit, the equations governing the motion relative to the system center of mass can be rewritten, introducing the effects of the eccentricity and electrodynamic forces as periodic forcing terms. These forcing terms change with the orbital period and prevent the existence of equilibrium positions along the local vertical.

Instead of equilibrium positions, the system has periodic orbits that have been studied numerically in this paper. To carry out the numerical analysis, we use an algorithm based on the Poincaré method of continuation of periodic orbits. The algorithm provides different families of periodic orbits and permits an exhaustive analysis when used together with the frequency entrainment law for periodically forced system.

We show the ability of the algorithm to obtain periodic orbits for an inert tether (i.e., without current) in elliptical orbits. These periodic orbits were detected in 1969 by Modi and Brereton,[6,7] for a general satellite. In the present analysis, they become part of a wider family of periodic orbits for the case of a tethered satellite. The algorithm also provides the stability properties of the new periodic orbits after having detected them.

We obtain the essential free parameters involved in the problem. But the main result of the analysis is to show the effects of the orbital eccentricity on the periodic orbits for the alive (i.e., with current) tether. The shape of the periodic orbits changes drastically from the circular to the elliptical case. The stability properties also change but in a more complex way.

Thus, when the eccentricity is small there are no qualitative changes in the stability properties of the periodic solutions, and both cases, circular end elliptic, turn out to be very similar. However, for increasing values of the eccentricity the dynamic instability becomes more and more pronounced. Beyond a critical value $e \approx 0.35$, the instability is very strong. Thus, the missions using orbits with very high eccentricity, $e \approx 0.5$–0.8, should face challenging control problems, if used with electrodynamic tethers.

The present analysis shows that the influence of the inclination i and the argument of the perigee ω are small, that is, these parameters change very slightly the effects of the orbital eccentricity e. Note, however, that the inclination i plays an important role, when $e = 0$, in the onset of the instability we are dealing with; in fact, if $i = 0$ the instability disappears.

To simplify the analysis, we introduced some assumptions that limit its validity, as, for example, a rigid tether model, a nontilted dipole model for the Earth magnetic field, damping and/or control are not considered and the tether current does not change along the orbit. This way, some interesting conclusions of general validity could be drawn. Obviously, the analysis must be improved in the future, removing some of the most restrictive assumptions. For instance, in an elliptical orbit it will be important to consider the variations of the tether current along the trajectory because of the differences in height between the apogee and the perigee. Because of the ionospheric plasma density, these differences produce important changes in the tether current, making the instability detected in this analysis smoother. However, such a detailed analysis should be attached to some tether configuration (bare tether, for example), and it is, by its own nature, of limited scope.

Acknowledgments

The contribution of Yago N. Andrés has been carried out during the academic year 2002/2003 as a research project entitled "Mecánica Orbital de Tethers Electrodinámicos. Simulación Dinámica." This work forms part of his doctorate training. The contribution of J. Peláez was carried out in the framework of the research project entitled "Estabilidad y Simulación Dinámica de Tethers" (BFM2001-3663), supported by the Dirección General de Investigación of the Spanish Ministry of Science and Technology.

References

[1]Peláez, J., Lorenzini, E. C., López-Rebollal, O., and Ruiz, M., "A New Kind of Dynamic Instability in Electrodynamic Tethers," *Spaceflight Mechanics 2000, Advances in the Astronautical Sciences*, Vol. 105, Pt. 2, 2000, pp. 1367–1386.

[2]Peláez, J., Lorenzini, E. C., López-Rebollal, O., and Ruiz, M., "A New Kind of Dynamic Instability in Electrodynamic Tethers," *Journal of the Astronautical Sciences*, Vol. 48, No. 4, 2000, pp. 449–476.

[3]Peláez, J., and Lara, M., "Periodic Solutions in Electrodynamic Tethers on Inclined Orbits," *Journal of Guidance, Control, and Dynamics*, Vol. 26, No. 3, 2003, pp. 395–406.

[4]Dobrowolny, M., "Lateral Oscillations of an Electrodynamic Tether," *Journal of the Astronautical Sciences*, Vol. 50, No. 2, 2002, pp. 125–147.

[5]Peláez, J., López-Rebollal, O., Lara, M., and Ahedo, E., "Dynamic Stability of a Bare Tether as a Deorbiting Device," American Astronautical Society, Paper AAS02-200, Jan. 2002.

[6]Modi, V. J., and Brereton, R. C., "Periodic Solutions Associated with Gravity-Gradient-Oriented Systems: Part I. Analytical and Numerical Determination," *AIAA Journal*, Vol. 7, No. 7, 1969, pp. 1217–1225.

[7]Modi, V. J., and Brereton, R. C., "Periodic Solutions Associated with Gravity-Gradient-Oriented Systems: Part II. Stability Analysis," *AIAA Journal*, Vol. 7, No. 8, 1969, pp. 1465–1468.

[8]Lara, M., and Peláez, J., "On the Numerical Continuation of Periodic Orbits: An Intrinsic, 3-Dimensional, Differential, Predictor-Corrector Algorithm," *Astronomy and Astrophysics*, Vol. 389, No. 2, July II, 2002, pp. 692–701.

[9]Fujii, Hironori A., Ichiki, Wakano, Suda, Shin-ichi, and Watanabe, Takeo R., "Chaos Analysis on Librational Control of Gravity-Gradient Satellite in Elliptic Orbit," *Journal of Guidance, Control, and Dynamics*, Vol. 23, No. 1, 2000, pp. 145, 146.

[10]Gulyaev, V. I., and Zubritskaya, A. L., and Koshkin, V. L., "Universal Sequence of Bifurcation of Doubling of the Oscillation Period for a Satellite in an Elliptical Orbit," *Mechanics of Solids*, Vol. 24, No. 3, 1989, pp. 1–6.

[11]Petrov, A. L., Sazonov, V. V., and Sarychev, V. A., "Stability of Periodic Oscillations of a Quasi-Axisymmetric Satellite in the Plane of an Elliptical Orbit," *Mechanics of Solids*, Vol. 18, No. 4, 1983, pp. 37–47.

[12]Demin, V. G., and Singkh, R. B., "Nonlinear Plane Oscillations of a Satellite in an Elliptical Orbit," *Cosmic Research*, Vol. 11, No. 2, 1973, pp. 172–176.

[13]Barkin, Yu. V., and Pankratov, A. A., "Periodic Motions of an Axisymmetric Satellite with Respect to Its Center of Mass in an Elliptical Orbit," *Cosmic Research*, Vol. 15, No. 4, 1977, pp. 453–459.

[14]Sarychev, V. A., Sazonov, V. V., and Zlatoustov, V. A., "Periodic Oscillations of a Satellite in the Plane of an Elliptical Orbit," *Cosmic Research*, Vol. 15, No. 6, 1977, pp. 698–719.

[15]Beletskii, V. V., *Motion of an Artificial Satellite About Its Center of Mass*, Mechanics of Space Flight, Israel Program for Scientific Translation, NASA & NSF, Jerusalem, 1966, Chap. 2 (translated from Russian).

[16]Siegel, C. L., and Moser, J. K., *Lectures on Celestial Mechanics*, Classics in Mathematics, Springer-Verlag, Berlin, 1971, Chap. 3.

[17]Murdock, J. A., *Perturbations: Theory and Methods*, Classics in Applied Mathematics, Wiley, New York, 1991, Chap. 4.

[18]Peláez, J., and Lorenzini, E. C., "Libration Control of Electrodynamic Tethers in Inclined Orbit," American Astronautical Society, Paper AAS03-214, Feb. 2003; also *Journal of Guidance, Control, and Dynamics* (to be published).

[19]Peláez, J., and Lara, M., "Damping in the Dynamic Stability of Deorbiting Bare Tethers," *Advances in the Astronautical Sciences*, Vol. 114, Pt. 3, 2003, pp. 1647–1666.